Journal of The Electrochemical Society, 151 (9) C590-C593 (2004)
0013-4651/2004/151(9)/C590/4/$7.00 © The Electrochemical Society, Inc.

Comparative Study of Cu-Precursors for 3D Focused Electron Beam Induced Deposition

A. Luisier,[a] I. Utke,[a,z] T. Bret,[a] F. Cicoira,[a] R. Hauert,[b] S.-W. Rhee,[c,*] P. Doppelt,[d,*] and P. Hoffmann[a]

[a]*Institute of Imaging and Applied Optics, School of Engineering, Swiss Federal Institute of Technology, CH-1015 Lausanne-EPFL, Switzerland*
[b]*EMPA Dübendorf, CH-8600 Dübendorf, Germany*
[c]*Laboratory for Advanced Molecular Processing, Department of Chemical Engineering, Pohang University of Science and Technology, San 31 Hyoja-dong, Nam-gu, Pohang, Kyungbuk 790-784, Korea*
[d]*Ecole Supérieure de Physique et Chimie Industrielles-CNRS, 75231 Paris Cedex 05, France.*

The copper precursors bis-hexafluoroacetylacetonato-copper $Cu(hfac)_2$, vinyl-trimethyl-silane-copper(I) hexafluoroacetylacetonate (hfac)Cu(VTMS), 2-methyl-1-hexen-3-yne-copper hexafluoroacetylacetonate (hfac)Cu(MHY), and dimethylbutenecopper(I) hexafluoroacetylacetonate (hfac)Cu(DMB) are compared with respect to deposition rates and metal content obtained by focused electron beam induced deposition. Exposure was performed with 25 keV electrons in a Cambridge S100 scanning electron microscope equipped with a lithography system. Tip deposition rates increase with increasing precursor vapor pressure and range between 47 nm/s for (hfac)Cu(DMB) to about 4 nm/s for $Cu(hfac)_2$. A decay of deposition rates with time, *i.e.*, tip length, is observed. Electric four-point measurements indicate an insulating behavior of deposited lines for all precursors. In contrast, Cu contents of up to 45-60 atom % were found by Auger electron spectroscopy in thin rectangular deposits using (hfac)Cu(DMB) and (hfac)Cu(VTMS) as precursors. A discussion in terms of monolayer coverage, completeness of precursor molecule dissociation, and precursor stability is presented.
 [DOI: 10.1149/1.1779335]

Manuscript submitted October 15, 2003; revised manuscript received February 16, 2004. Available electronically August 11, 2004.

Due to its superior electrical conductivity over Al or W, Cu is being implemented as standard in high performance integrated circuits in microelectronics. Scanning electron microscopy (SEM) failure analysis combined with focused electron beam (FEB) induced writing would offer a powerful important tool for *in situ* rewiring of circuit defects. FEB induced writing is essentially a local chemical vapor deposition (CVD) process. Decomposition is achieved by interaction of electrons with surface adsorbed molecules and results in three-dimensional (3D) growth. Controlling the electron beam with a lithography program allows writing almost all kind of nanostructures from dots, lines, tips, and periodic patterns to sophisticated structures with high precision and resolution. According to the precursors used deposit properties can be tuned to different applications like thermal nanoprobes,[1] nanotweezers,[2] field-emitters,[3,4] magnetic force microscopy tips,[5] atomic force microscopy tips[6,7] circuit reparation,[8] mask repair, etch masks,[9] and nanoantennae on scanning near field optical fiber probes.[10]

In this study we compare different copper precursors, shown in Fig. 1, for their suitability in FEB induced writing with respect to their deposition rates and the deposit metal content: $Cu(II)(hfac)_2$ (hfac: hexafluoroacetylacetonate), (hfac)Cu(I)(MHY) (MHY: 2-methyl-1-hexen-3-yne),[11] (hfac)Cu(I)(VTMS) (VTMS: vinyltrimethylsilane), and (hfac)Cu(I)(DMB) (DMB: dimethylbutene).[12] It can be seen from Table I that these precursors differ considerably in vapor pressure determining the precursor molecule flux for FEB deposition. Precursor flux values at the nozzle exit in Table I were estimated using the transient flow theory developed by Dushman.[13] The dissociation temperature of the ligands determined by thermogravimetry and the CVD temperature indicate the chemical stability of the precursor complex. The Cu:C stoichiometry in these precursors varies slightly between 0.08-0.1.

Experimental

A schematic of the experimental setup is shown in Fig. 2. Naturally oxidized Si was used as substrate. A steel tube centred with the electron beam, supplies the precursor from an internal metal reservoir. This supply was used for all precursors. Precursor filling was accomplished within a glove box under dry nitrogen atmosphere. FEB exposure was performed with 25 keV electrons in a Cambridge S100 scanning electron microscope (SEM). Deposition rates were determined from vertical tip series produced with the SEM spot mode at 500 pA corresponding to a measured electron beam diameter ($1/e^2$) of 132 nm. The deposits were analyzed *ex situ* with respect to their geometry in a SEM (FEG XL30). The deposition rate was taken as length interval divided by exposure time interval. Composition analysis was performed on $5 \times 7\ \mu m^2$ large and about $1\ \mu m$ thick rectangles deposited at 1 nA using the SEM scan mode. Sputter profiling Auger electron spectroscopy (AES) was performed with two different conditions of probe current I_p and probe energy E_p; (a) $I_p = 75$ nA and $E_p = 5$ kV (PHI 4300) and (b) $I_p = 5$ nA and $E_p = 3$ kV (PHI 660-EPFL). Line deposits of about $60\ \mu m$ length were written with a Nabity lithography system on SiO_2 (150 nm)/Si substrates with lift-off gold electrodes for four-point electrical resistivity measurements (HP 4156A precision semiconductor parameter analyzer).

Results and Discussion

Figure 3 shows that the initial deposition rate increases with increasing precursor vapor pressure, *i.e.*, increasing precursor flux. The differing initial deposition rates can be related to the initial surface monolayer coverage θ using Langmuir's isotherm, according to which

$$\theta = bP/(1 + bP) \tag{1}$$

The thermodynamic parameter b describes the surface adsorption/desorption behavior and P is the local pressure above the sample being proportional to the precursor flux reported in Table I. From their similar molecular structures, the Cu(I) precursors can be supposed to have similar thermodynamic behavior, *i.e.*, $b_{VTMS} \approx b_{DMB} \approx b_{MHY}$, and electron dissociation cross sections. In other words, the initial growth rates R_0 would depend only on the amount θ of precursor adsorbed at the surface. The ratios $R_{0,DMB}:R_{0,VTMS} = 47:20$ (see Fig. 2A), and $P_{DMB}:P_{VTMS} = 30$ (from Table I) lead to monolayer coverages of $\theta_{VTMS} = 40.6\%$ and $\theta_{DMB} = 95.3\%$. The value for (hfac)Cu(VTMS) agrees well with the value of 2×10^{14} molecules/cm^2 reported in Ref. 14. Agreement is also

* Electrochemical Society Active Member.
z E-mail: Ivo.Utke@epfl.ch

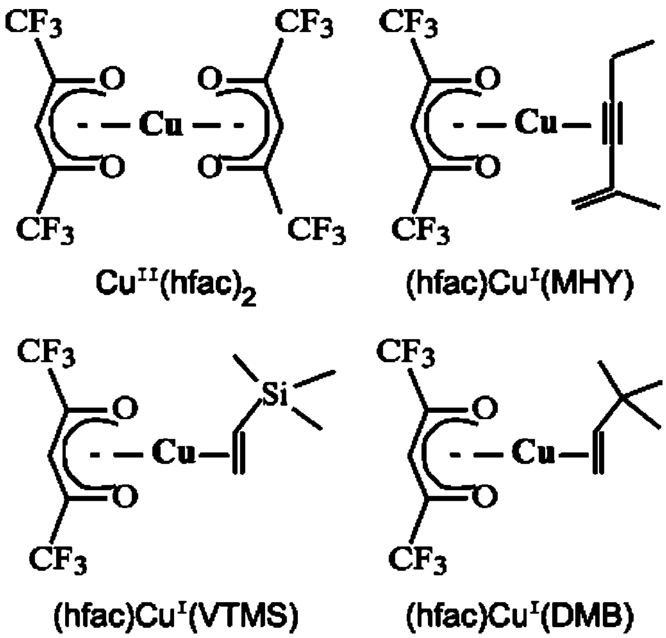

Figure 1. Chemical formulas of Cu precursors used in our comparative study.

found for $\theta_{\mathrm{MHY}} = 57.6\%$ and the initial deposition rate ratio $R_{0,\mathrm{VTMS}}:R_{0,\mathrm{MHY}} \approx \theta_{\mathrm{VTMS}}:\theta_{\mathrm{MHY}}$. For the Cu(II) precursor $\mathrm{Cu(hfac)_2}$, the coverage is estimated to $\theta_{\mathrm{hfac}} = 2.4\%$ which should result in an initial deposition rate of about 1 nm/s, whereas 4 nm/s are observed experimentally. The parameter b of this Cu(II) compound may be larger with respect to the (hfac)Cu(I)-L family, due to stronger interactions of the surface with the more accessible out-of-plane Cu *d* orbitals, thus intuitively justifying the discrepancy.

All precursors then show a decay of deposition rate with time (increasing tip length) inversely correlated to their initial growth rate, that is, most pronounced for (hfac)Cu(DMB), comparable for (hfac)Cu(VTMS) and (hfac)Cu(MHY), and smallest for $\mathrm{Cu(hfac)_2}$. The deposition rate saturates at a certain minimum value depending on the precursor, although it is not reached for all precursors within the investigated time interval (0-20 min). The same effect has been observed with other metallorganic precursors.[15]

We can discuss three mechanisms for this observation. The first mechanism involves thermal effects induced by electron irradiation on a poor heat conducting tip deposit. It was recently shown by energy dispersive X-ray spectroscopy that free-standing horizontal copper rod deposits made from (hfac)Cu(VTMS) contain all precursor elements, *i.e.*, Cu, Si, F, O, and C. However, these rods transform into almost pure copper-rods with coalesced nanocrystals of up to 100 nm in size after additional irradiation and vertical tip growth on top of them.[16] As shown in the Monte Carlo simulation inset of Fig. 3B, the primary electrons lose part of their energy before being scattered out of the apex cone region. Experimental support of the simulated electron trajectories can be found by *in situ* monitoring

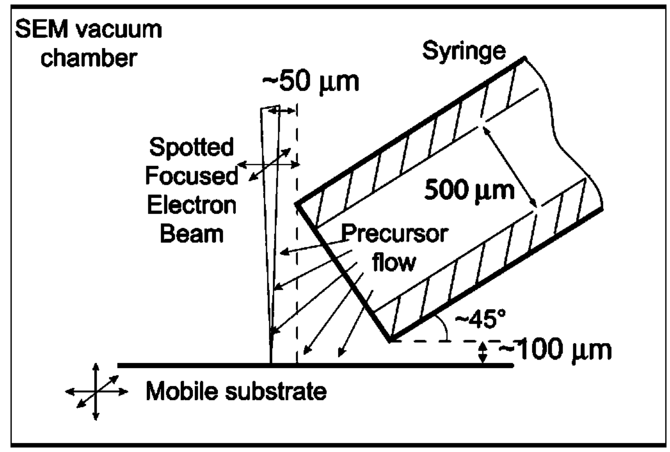

Figure 2. Schematics of the experimental setup.

the substrate current and secondary electron emission during growth, as recently reported in Ref. 17. The tip apex gets hotter due to decreasing heat dissipation with increasing tip length, *i.e.*, the precursor molecules desorb faster and the deposition rate decays. Taking 100°C as dissociation temperature (see Table I), a rough estimation of the thermal conductivity similar to the one outlined in Ref. 18 gives for the above-mentioned rods a value of about 2 W/mK, which is about 10 times better than PMMA but about 200 times worse than pure copper (395 W/mK). The bad electrical conductivity of our deposits supports this estimation. The second mechanism would concern the precursor supply by surface diffusion due to concentration gradients between a locally FEB-depleted zone and the surrounding adsorbates. With increasing tip length the diffusion source changes from two-dimensional (substrate) to one-dimensional (tip cylinder wall) reducing the available precursor at the tip apex region. The cylinder wall is continuously replenished with new molecules from the gas phase whereas molecules from the substrate source are fixed around the tip base by tip-scattered primary electrons (and their generated secondary electrons), see inset in Fig. 2B. Decay and saturation of the growth rate could be explained with this mechanism. However, it would fail to explain the above-mentioned formation of pure copper crystals.

The third mechanism could rely on the assumption that at small electron/precursor flux-ratios less electrons are available for molecule decomposition and that fragmentation becomes increasingly incomplete. Because the tip grows coaxially into the electron beam, electrons can still fragment the tip material inside the cone region, which would densify the fast-grown deposits. However, this should result in constant growth rates after the cone formation, *i.e.*, after 0.8 µm tip length for all precursors, which is not observed here.

The time dependence of the deposition rate can be used to write different line structures with a single slow scan as shown in Fig. 4. If the scan speed is sufficiently large with respect to the vertical deposition rate, the deposit will evolve into a line attached to the substrate as shown in Fig. 4A. If both are comparable, the deposits take off with an angle of about 45°. The continuously decreasing

Table I. Summarized precursor properties: vapor pressure (P_{vap}), estimated flux at nozzle exit, ligand dissociation temperature (T_{diss}), and minimum CVD temperature (T_{min}) to obtain films with electrical resistivity <2.5 µΩ cm.

Precursor	P_{vap} at 25°C (mbar)	Precursor flux (no./cm^2 s)	T_{diss} (°C)	T_{min} CVD (°C)	Cu:C ratio	Ref.
$\mathrm{Cu(hfac)_2}$	0.004	3.5×10^{16}	—	250	1:10	19
(hfac)CuVTMS	0.1	1×10^{18}	63	100	1:10	20
(hfac)CuMHY	0.2	2×10^{18}	207	180	1:11	21, 22
(hfac)CuDMB	1.3	3×10^{19}	88	125	1:12	20

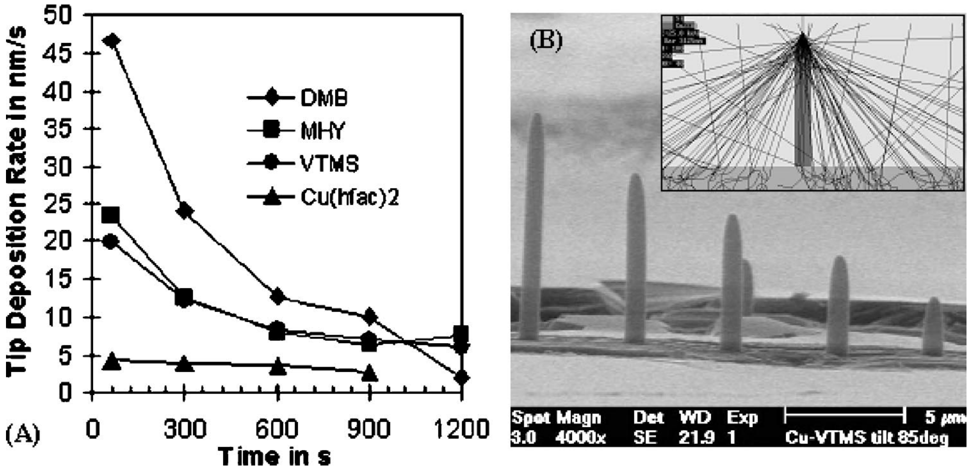

Figure 3. (a) Comparison of deposition rates of different Cu precursors. (b) Scanning electron micrograph of Cu tips grown at 25 kV and 500 pA with (hfac)Cu-(VTMS) on Si substrate with varying exposure time. The inset shows Monte Carlo simulated electron trajectories for one tip deposit (same scale as image): electron energy 25 keV, tip composition and density set to Cu_2C_8 and 4.2 g/cm^3 on Si substrate.

vertical deposition rate superposed with the constant lateral scan speed evolves into a horizontal rod shape. When the focused electron beam partially advances in front of the deposit or gets transmitted through the horizontal rod end volume it hits again the substrate and a new deposit starts. This mechanism produces ''freestanding'' lines with a periodic pattern as shown in Fig. 4B, which can be tuned by the scan speed. Line resistivity measurements indicate an insulating behavior independent of the precursor used. Improved conductivity may be obtained by variation of *in situ* parameters like addition of reactive gases or further *ex situ* treatments of the deposits, for instance H_2-plasma to turn their composition to pure Cu. We do not focus here on this topic but consider in more detail the chemical outcome of the process, depending on the precursor used.

Auger electron spectroscopy (AES) measurements in thin rectangular deposits are summarized in Table II. All deposits contain Cu in a higher amount than present in the corresponding precursor, however, not related to the precursor stoichiometry (Cu:C ratio) as reported in Table I. Both, (hfac)Cu(MHY) and $Cu(hfac)_2$, show relatively low but stable composition values in the bulk, *i.e.*, during sputtering cycles. Higher Cu content is found for (hfac)Cu(DMB) and (hfac)Cu(VTMS) but values fluctuate strongly after the consecutive Ar ion sputtering cycles. We begin the interpretation of these results by looking at the thermal decomposition mechanism of copper(I) precursors, which often proceeds by the following disproportion reaction[19]

$$2[(hfac)Cu(I)(L)] \rightarrow Cu(0) + Cu(II)(hfac)_2\uparrow + 2L\uparrow \quad [2]$$

where L = VTMS, DMB, or MHY. Thus $Cu(hfac)_2$ is the most stable precursor in our study and its CVD temperature range is the highest among our precursors, see Table I. Furthermore, according to the temperatures needed to dissociate L from the molecule[19-22] the precursor stability order can be established to $Cu(hfac)_2$ > (hfac)Cu(MHY) > (hfac)Cu(DMB) > (hfac)Cu(VTMS). Supposing that a more stable molecule will need an increased number of electrons to get fragmented into Cu and organic species, the FEB deposit metal content should thus increase $Cu(hfac)_2$ < (hfac)Cu(MHY) < (hfac)Cu(DMB) < (hfac)Cu(VTMS). This precursor stability-based order is obtained by AES except for the last two precursors, the composition of which however largely fluctuates during depth profiling. As noted above, at large precursor fluxes, *i.e.*, small electron/precursor flux ratios, the fragmentation is incomplete and a nonvolatile carbon-rich matrix grows from polymerization of remaining ligands. The electron/precursor flux ratio (primary electrons/molecule) reported in Table II hence suggests an inverse order of metal content of deposits than that obtained by the precursor stability. Because both mechanisms counteract, they could approximately outbalance and result in about the same low Cu-contents for all deposits. This is at least supported by the electrical measurements, which resulted in insulating behavior for all deposits. It remains the question why AES gives much higher Cu-content values for (hfac)Cu(DMB) and (hfac)Cu(VTMS). The largely fluctuating value of both precursors leads us to the assumption that the electron/ion exposure during sputter cycle Auger measurements probably alters these deposits. Moreover, the etching rate of incompletely reticulated carbonaceous species could be larger during sputtering than that of copper and dense carbon polymers, leading to an increase in the Cu proportion. The minimum value of the AES measured Cu content should thus be closer to the original FEB decomposition whereas the maximum value should correspond to the postdecomposition/etching induced from the inspection itself. No measurable postdecomposition/etching takes place for the more stable precursors $Cu(hfac)_2$ and (hfac)CuMHY for which the Cu/C ratio of 1:5 to 1:6 is maintained throughout the measurement/sputter cycles. Hence decomposition of these precursors and reticulation of the remaining carbonaceous species seems to be complete which goes along with the estimated high electron/precursor flux ratios of 55-1500 for these precursors.

In this context it should be noted that XPS measurements show considerable lower Cu contents in (hfac)CuVTMS deposits by FEB than AES. This was discussed as a result of weaker interaction of

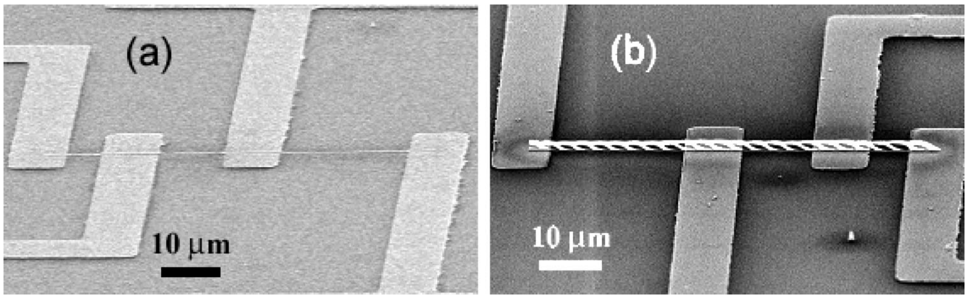

Figure 4. Tilt SEMs of FEB (25 kV, 500 pA, single scan with scan speed of 35 nm/s) deposits for four-point electrical measurements on lift-off gold electrodes on SiO_2/Si substrate. Distance between the two outermost electrodes is 55 μm. (a) Line deposited with (hfac)Cu(VTMS). (b) 3D freestanding line grown by a single scan with (hfac)Cu(DMB).

Table II. Chemical composition measured by AES of FEB deposits at room temperature from different Cu precursors and estimation of the electron/precursor flux ratio (electron flux 5.5 $\times$ 10^{19} cm^{-2} s^{-1} at 500 pA and 25 kV). The fluorine signal was not significantly above the noise level of the AES measurements.

Precursors	Cu	C	O	Si	Flux-Ratio e^-/molecule
$Cu(hfac)_2$	14	75	5	—	1500
(hfac)CuMHY	13	82	3	—	55
(hfac)CuVTMS	20-45	35-70	8-14	2-10	28
(hfac)CuDMB	25-60	15-60	5-25	—	2

X-rays[23] and supports the mechanism of a postdecomposition/etching process of a polymerized matrix induced by AES as discussed above.

Conclusions

We presented a comparative study of Cu precursors for FEB induced deposition. The initial deposition rate could be related to the monolayer coverage according to Langmuir's adsorption isotherm. Deposit compositions in this study were not dependent on the Cu/C-ratio of the precursor. The deposit Cu content was experimentally shown to decrease with increasing precursor stability. With electron/precursor flux ratios $<$55, being below the electron decomposition efficiency complete dissociation seems not to be achieved as indicated by AES values fluctuating within 15-70 atom % for Cu. The maximum value also indicates that the low-stability precursors (hfac)Cu(DMB) and (hfac)Cu(VTMS) have a great potential for high conductivity deposits useful for local *in situ* microcircuit repair, when deposited by FEB under high electron/precursor flux-ratio conditions.

The Swiss Federal Institute of Technology assisted in meeting the publication costs of this article.

References

1. K. Edinger, T. Gotszalk, and I. W. Rangelow, *J. Vac. Sci. Technol. B*, **19**, 2856 (2001).
2. P. Bøggild, T. M. Hansen, C. Tanasa, and F. Grey, *Nanotechnology*, **12**, 331 (2001).
3. H. W. P. Koops, C. Schossler, A. Kaya, and M. Weber, *J. Vac. Sci. Technol. B*, **14**, 4105 (1996).
4. M. Takai, T. Kishimoto, H. Morimoto, Y. K. Park, S. Lipp, C. Lehrer, L. Frey, H. Ryssel, A. Hosono, and S. Kawabuchi, *Microelectron. Eng.*, **41-42**, 453 (1998).
5. I. Utke, R. Berger, L. Scandella, and P. Hoffmann, *Appl. Phys. Lett.*, **80**, 4792 (2002).
6. Y. Akama, E. Nishimura, A. Sakai, and H. Murakami, *J. Vac. Sci. Technol. A*, **8**, 429 (1990).
7. B. Hubner, H. W. P. Koops, H. Pagnia, N. Sotnik, J. Urban, and M. Weber, *Ultramicroscopy*, **42**, 1519 (1992).
8. I. Utke, B. Dwir, K. Leifer, F. Cicoira, P. Doppelt, P. Hoffmann, and E. Kapon, *Microelectron. Eng.*, **53**, 261 (2000).
9. K. T. Kohlmann von Platen, L. M. Buchmann, H. C. Petzold, and W. H. Bruenger, *J. Vac. Sci. Technol. B*, **10**, 2690 (1992).
10. O. Sqalli, I. Utke, P. Hoffmann, and F. Marquis-Weible, *J. Appl. Phys.*, **92**, 1078 (2002).
11. T. Y. Chen, J. Vaissermann, E. Ruiz, J. P. Senateur, and P. Doppelt, *Chem. Mater.*, **13**, 3993 (2001).
12. S.-W. Rhee, S.-W. Kang, and S.-H. Han, *Electrochem. Solid-State Lett.*, **3**, 135 (2000).
13. S. Dushman, in *Scientific Foundations of Vacuum Technique*, J. M. Lafferty, Editor, J. Wiley & Sons, New York (1962).
14. T. P. Chiang, H. H. Sawin, and C. V. Thompson, *J. Vac. Sci. Technol. A*, **15**, 3104 (1997).
15. H. W. P. Koops, M. Rudolph, J. Kretz, and M. Weber, in *Nanolithography: A Borderland Between STM, EB, IB, and X-Ray Lithographies*, M. Gentili, Editor, p. 87, Kluwer Academic Publishers, The Netherlands (1994).
16. I. Utke, A. Luisier, P. Hoffmann, P. A. Buffat, and D. Laub, *Appl. Phys. Lett.*, **81**, 3245 (2002).
17. T. Bret, I. Utke, A. Bachmann, and P. Hoffmann, *Appl. Phys. Lett.*, **83**, 4005 (2003).
18. I. Utke, T. Bret, D. Laub, Ph. Buffat, L. Scandella, and P. Hoffmann, *Microelectron. Eng.*, *In press.*
19. T. Kodas and M. Hampden-Smith, in *The Chemistry of Metal CVD*, VCH Verlagsgesellschaft GmbH, Weinheim (1994).
20. K. K. Choi and S. W. Rhee, *Thin Solid Films*, **409**, 147 (2002).
21. T. Ohta, Unpublished results.
22. P. Doppelt, *Coord. Chem. Rev.*, **180**, 1785 (1998).
23. S. Mezhenny, I. Lyubinetsky, W. J. Choyke, and J. T. Yates, *J. Appl. Phys.*, **85**, 3368 (1999).